Abstract #: 753
Program #: PS-ThM7
Put on JVST manuscript



# Potential applications of an electron cyclotron resonance multicusp plasma source*

C. C. Tsai, L. A. Berry, S. M. Gorbatkin, H. H. Haselton, J. B. Roberto, and W. L. Stirling

Oak Ridge National Laboratory, Oak Ridge, Tennessee 37831



## ABSTRACT

An electron cyclotron resonance (ECR) multicusp plasmatron has been developed by feeding a multicusp bucket arc chamber with a compact ECR plasma source. This novel source produces large (about 25-cm-diam), uniform (to within ±10%), dense (>$10^{11}$-$cm^{-3}$) plasmas of argon, helium, hydrogen, and oxygen. It has been operated to produce an oxygen plasma for etching 12.7-cm (5-in.) positive photoresist-coated silicon wafers with uniformity within ±8%. Results and potential applications of this new ECR plasma source for plasma processing of thin films are discussed.



---

*Research sponsored by the U.S. Department of Energy under contract DE-AC05-84OR21400 with Martin Marietta Energy Systems, Inc.

# I. INTRODUCTION

Plasma ion sources[1–5] are useful for isotope separation, space propulsion, fusion plasma heating, ion-beam materials processing, plasma processing, etc. As the heart of such an ion source, the plasma source for a particular application must provide the needed current density, electron temperature, plasma uniformity, and ion species. It should also be compact, simple, flexible, reliable, and efficient.

The needs of the multi-megawatt neutral beam injectors used to heat fusion plasmas[3] drove much early ion source development. The duoPIGatron ion source,[6] developed at Oak Ridge National Laboratory (ORNL) in the 1960s, was the basis of ion sources that have produced pulsed ion beams of hydrogen isotopes with currents ≤ 100 A, energies > 100 keV, pulse lengths ≤ 30 s, and duty factors ≤ 10%. The large plasma sources produced uniform plasmas with densities of $>10^{12}$ $cm^{-3}$ over areas approaching 1000 $cm^2$.

The original duoPIGatron ion source[7] injected 600-keV, 0.5-A dc hydrogen ion beams. Intensive studies of plasma production, ion beam formation,[8] and source operating mechanisms[9] led to currents > 10 A. The application of multicusp magnetic field confinement produced more uniform plasmas,[10,11] as shown in Fig. 1 for a 15-cm duoPIGatron ion source.[12]

The combination of the duoPIGatron plasma source, optimized electrode geometry, and multicusp confinement yielded plasma sources that produced dense, uniform 15- to 30-cm-diam plasmas with circular or rectangular cross sections, which uniformly extended to ≈5 cm from the walls of the bucket chamber . These modified duoPIGatron ion sources[12–16] were scaled up to produce pulsed ion beams with currents up to 100 A, as shown in Fig. 2. The 100-A modified duoPIGatron ion source (Fig. 3 ) was developed at ORNL in 1978 for both the Poloidal Divertor Experiment at Princeton Plasma Physics Laboratory and the Impurity Study Experiment at ORNL.

The source plasma in a duoPIGatron consists of a cathode plasma and an anode plasma. The cathode plasma is produced by primary electrons emitted from hot filaments; the anode plasma, by

electrons extracted from the cathode plasma and accelerated into the anode region. The anode plasma is confined in the multicusp "bucket" chamber. The spatial uniformity of the dense anode plasmas is optimized by varying the neutral gas feed, the solenoid magnet current, and the arc power. Radial density profiles for these (1–2) × $10^{12}$-$cm^{-3}$ plasmas are nearly flat, as shown in Fig. 4 for a 30-cm-diam ion source[15] that produced up to 100 A of hydrogen ions at 50 kV.

The impurity content[17] of the hydrogen ion beams produced by these sources is very low, because impurity ions are produced only in the cathode plasma region. Thus, these sources are ideal for plasma materials processing. However, their thermionic cathodes can be attacked by reactive-gas plasmas, they have other compatibility problems with reactive gases, and their lifetimes are relatively short. Electron cyclotron resonance (ECR) microwave plasma generation eliminates cathode limitations and has been widely used[18–20] to achieve high plasma densities in low-pressure reactive gases. We have developed an ECR multicusp plasmatron by feeding a multicusp bucket chamber with plasmas produced by a compact ECR source,[21] as shown in Fig. 5.

## II. ORNL ECR MULTICUSP PLASMATRON

The ECR plasma source has been developed primarily from existing components for the 20-cm duoPIGatron,[14] except for the microwave launcher. The axial solenoid magnet (11.4-cm i.d., 17.2-cm o.d., 7.1 cm long, with 64 turns) that surrounds the microwave launcher provides the 875-G field needed to establish an ECR zone for 2.45-GHz microwaves. At the center of the solenoid, a commercial MDL glass/Kovar pressure window (model 284WD56) provides a vacuum-tight seal with the standard S-band waveguide. For data in this paper, a matching network was not used. Figure 6 shows how this ECR zone can be dynamically moved from the central plane of the magnet by varying the excitation current applied to the magnet. On the outside walls of the 30-cm-diam, 20-cm-high plasma chamber, 20 permanent magnet columns with alternating

polarity form the multiple-line cusp configuration that confines the plasma. A secondary ECR zone is established in this multicusp field region near the chamber walls.

The launcher has the same dimensions as the S-band waveguide. Microwave energy is launched from the high-field region and propagates in the direction parallel to the source magnetic field lines. The microwave power $P_{\mu}$, applied magnetic field $B_{applied}$, gas type, throughput, and gas pressure $p$ strongly affect the plasma density and uniformity. However, for any operating pressure or flow rate (throughput), the spatial uniformity can be optimized by adjusting $B_{applied}$ and $P_{\mu}$.

## III. SOURCE OPERATION

The source has been operated with argon, oxygen, helium, and hydrogen. The operating pressure limit, above which an ECR discharge can be reliably established, is determined by the differential ionization coefficient of a gas; the higher this coefficient, the lower the pressure limit. The pressure limits for oxygen and argon are lower than those for hydrogen and helium. However ECR plasmas created with different gases respond similarly to the effects of $p$, $P_{\mu}$, $B_{applied}$, and substrate biasing. The source plasma normally has electron densities of up to $1 \times 10^{11}$ cm$^{-3}$, cold electron temperatures of 2 to 5 eV, ion energies of about 20 eV, and a production efficiency near 300 W/A (300 eV/ion).

As shown in Fig. 7, where the radial density distribution of a hydrogen plasma is plotted vs $p$ the source can create uniform (within 10%) plasmas over 24 cm in diameter. However, for constant $B_{applied}$ and $P_{\mu}$, these plasmas can be produced only within a narrow range of hydrogen pressures near 8.8 mTorr. For constant pressure and input power, we observe that (1) the plasma density increases with $B_{applied}$ ; (2) discharges that produce plasmas with peaked profiles near the axis tend to have high reflecting voltage or power; and (3) discharges that produce plasma with severely hollow profiles tend to have low reflecting voltage or power.

The plasma density and the reflected power increase as the pressure increases, as shown in Fig. 8 for argon plasmas. The ratio of reflected voltage to forward voltage is >50% in argon plasmas, compared with 10–20% in hydrogen plasmas, because of argon's higher ionization coefficient and the resulting higher plasma density in the microwave launcher. With argon or oxygen, plasma production rates are higher in the primary ECR zone and lower in the secondary ECR zone than they are for hydrogen under similar conditions. The resulting high plasma density inside the launcher increases the reflected power or voltage.

Plasmas can be created at lower pressures if a substrate is electrically floated or biased negatively, possibly because the hot electrons are reflected from the substrate and are more likely to produce plasma before escaping to the chamber walls. With biasing, a fairly uniform oxygen plasma can be created at 3 mTorr; a typical spatial profile is shown in Fig. 9.

The launcher configuration also affects the plasma density, uniformity, and efficiency. The rectangular launcher has recently been converted into a tapered launcher. The new geometry should reduce the loss of hot electrons to the launcher walls and result in higher efficiency; some of the hot electrons will drift to the bucket chamber and produce plasma there.

## IV. HYPOTHETICAL DISCHARGE MODEL

The strong pressure dependence shown in Fig. 7 can be understood in terms of simple wave propagation and absorption phenomena. At lower pressures, the plasma density in the launcher is below the ordinary-mode cutoff of $7.5 \times 10^{10}$ cm$^{-3}$. Left-hand circularly polarized (LHCP) microwaves are not absorbed at the primary ECR zone but are transmitted through it and absorbed at the secondary ECR zone, increasing the plasma density there. Many of the field lines from the primary ECR zone intersect the walls of the launcher, so many of the energetic electrons hit these walls. Thus, plasma production in the center of the plasma chamber is suppressed, even though the right-hand circularly polarized (RHCP) wave should couple very efficiently to this region. These

effects produce a hollow profile. As $p$ is increased, plasma generation by the RHCP wave at the primary ECR zone increases proportionally, and the profiles fill in and become peaked. At the resulting higher central plasma density (most likely above cutoff), the LHCP wave is reflected back into the microwave generator, and plasma production in the cusp field region is substantially reduced. The increase in reflected power at higher operating pressures and the absolute decrease in plasma density at the plasma edge are consistent with this hypothesis.

Plasma production by the LHCP wave in the secondary ECR zone is enhanced by the effective confinement in the multicusp configuration of the hot electrons, which could gain energy in the primary ECR zone. These electrons contribute to plasma production near the bucket walls, thus increasing the difference in plasma production rates in the two ECR zones. The cusp field in the secondary ECR zone confines the plasma electrons and minimizes the loss of plasma to the side walls.

The secondary ECR zone can also explain the difference in edge density gradients observed in a conventional duo Pig antenna and the ECR system. In a conventional duoPIGatron, the uniform plasma extends only to 5 cm from the chamber walls. In the ECR source, as shown in Fig. 7, it can extend to ≈3 cm from the walls. This could result from the additional plasma production in the secondary ECR zone. However, $p$ (or the neutral particle density) in each ECR zone directly affects the plasma production. Even with dc gas feed distributed on the top flange of the plasma chamber, the plasma production rate in each zone is a sensitive function of $p$, as noted in Sec. III.

At higher magnetic fields (see Fig. 6), the primary ECR zone lies closer to the exit from the launcher, and less plasma will be created inside the launcher. This reduction in plasma production may result in lower plasma densities in the launcher and the immediate vicinity of the exit, thus, increasing the transmission of the LHCP. Consistent with this model, reduced axial plasma densities and increased secondary ECR of plasma production are often seen as B is increased, especially for higher pressures. Again in this case, larger reflected power levels are correlated with peaked density profiles.

## V. RESULTS OF PLASMA ETCHING

We have exposed 12.7-cm-diam (5-in.-diam) silicon wafers coated with positive photoresist to oxygen plasmas created with the ECR microwave source. Figure 10 shows the resulting etch profiles via optical measurements done by Holber and Yeh[21]. The etching rate of 0.15 μm/min was uniform to within 15% over the 12.7-cm diameter. In practice, etching rates can be affected by local particle energy, particle ions and excited neutrals, and particle flux. The consistency of the etching profiles (Fig. 10) attests to the uniformity of the plasma produced by the ECR source (Fig. 9).

## VI. DISCUSSION

The ORNL ECR plasma source can produce plasmas with densities of up to $10^{11}$ $cm^{-3}$ and electron temperatures of <5 eV. This source has potential applications in thin-film deposition and etching, sputtering or ion implantation, and neutral beam heating for magnetic fusion plasmas.

To fulfil the requirements of a particular application, the source must be tailored to produce plasmas with the desired properties. For example, in microelectronic wafer processing a high degree of uniformity (variation of less than a few percent in spatial density) over a large diameter (≥20 cm) is desired. For fast, anisotropic etching, as required for submicrometer applications, high plasma density at low pressure (0.1 to 1 mTorr) is desirable to avoid gas phase scattering. Thus, the source parameters must be optimized to produce the best combination of etching rate, anisotropy, selectivity, and reproducibility.

ACKNOWLEDGMENTS

The plasma source development is carried out within the Fusion Energy and Solid State divisions of ORNL, with support from the Director's Exploratory Fund. The authors thank those who helped with this project, particularly W. Holber and J. Yeh of the Thomas J. Watson Research Center, who provided sample wafers for etching and analyzed the positive photoresist etching depth, and T. S. Bigelow, H. D. Kimrey, T. L. White, D. E. Schechter, F. Sluss, B. E. Argo, and G. C. Barber of ORNL.

This research was sponsored by the U.S. Department of Energy under contract DE-AC05-84OR21400 with Martin Marietta Energy Systems, Inc.

REFERENCES

[1]R. K. Wakerling and A. Guthrie, eds., *Electromagnetic Separation of Isotopes in Commercial Quantities* (U.S. Atomic Energy Commission, 1951).

[2]H. R. Kaufman, Adv. Electron. Electron Phys. **36**, 266 (1974).

[3]M. M. Menon, Proc. IEEE **69**, 1012 (1981).

[4]H. R. Kaufman, J. J. Cuomo, and J. M. E. Harper, J. Vac. Sci. Technol. **21**, 725 (1982).

[5]J. B. Roberto and L. A. Berry (private communication).

[6]G. G. Kelley, N. H. Lazar, and O. B. Morgan, Nucl. Instrum. Methods **10**, 263 (1961).

[7]O. B. Morgan, G. G. Kelley, and R. C. Davis, Rev. Sci. Instrum. **38**, 467 (1967).

[8]O. B. Morgan, in *Proc. 2nd Symp. Ion Sources and Formation of Ion Beams* (Lawrence Berkeley Laboratory, Berkeley, Calif.,1974), paper VI-1.

[9]C. C. Tsai, W. L. Stirling, and P. M. Ryan, Rev. Sci. Instrum. **48**, 651 (1977).

[10]R. David Moore, paper 69-260 presented at the AIAA 7th Electric Propulsion Conference, Williamsburg, Va., March 3–5, 1969.

[11]R. Limpaecher and K. R. MacKenzie, Rev. Sci. Instrum. **44**, 726 (1973).

[12]W. L. Stirling, C. C. Tsai, and P. M. Ryan, Rev. Sci. Instrum. **48**, 533 (1977).

[13]H. H. Haselton, D. E. Schechter, G. Schilling, L. A. Stewart, and W. L. Stirling, in *Proc. 6th Int. Symp. Engineering Problems of Fusion Research* (IEEE, New York, 1975), pp. 169–171.

[14]C. C. Tsai, W. L. Stirling, H. H. Haselton, R. C. Davis, and D. E. Schechter, in *Proc. 7th Int. Symp. Engineering Problems of Fusion Research* (IEEE, New York, 1977), pp. 278–283.

[15]W. L. Gardner, G. C. Barber, C. W. Blue, W. K. Dagenhart, H. H. Haselton, J. Kim, M. M. Menon, N. S. Ponte, P. M. Ryan, D. E. Schechter, W. L. Stirling, C. C. Tsai, J. H. Whealton, and R. E. Wright, Rev. Sci. Instrum. **53**, 424 (1982).

[16]M. M. Menon, C. C. Tsai, J. H. Whealton, D. E. Schechter, G. C. Barber, S. K. Combs,

W. K. Dagenhart, W. L. Gardner, H. H. Haselton, N. S. Ponte, P. M. Ryan, W. L. Stirling, and R. E. Wright, Rev. Sci. Instrum. **56**, 242 (1985).

[17]R. A. Langley and C. W. Magee, J, Nucl. Mater. 93/94 390 (1980)

[18]K. Suzuki, S. Okudaira, N. Sakudo, and I. Kanomata, Jpn. J. Appl. Phys. **16**, 1979 (1977).

[19]R. R. Burke and C. Pomot, Solid State Technol. **31** (2), 67 (1988).

[20]J. Asmussen, "Electron Cyclotron Resonance Microwave Discharge for Etching and Thin Film Deposition," Chap. 11 of *Plasma-Based Processing* (Noyes Publications, Park Ridge, N.J., in press.)

[21]L. A. Berry, S. M. Gorbatkin, J. B. Roberto, C. C. Tsai, W. Holber, and J. Yeh, "Characteristics of the ORNL ECR Multiple Plasma Source," presented at the SRC Topical Research Conference on Plasma Etching, Cambridge, Mass., February 1–2, 1989.

FIG. 1. Effect of multicusp confinement on plasma uniformity.

FIG. 2. Evolution of the modified duoPIGatron ion source at ORNL.

FIG. 3. 30-cm duoPIGatron ion source for forming 100 A of hydrogen ions.

FIG. 4. Typical radial profile of hydrogen plasma produced by the source shown in Fig. 3.

FIG. 5. ECR multicusp plasmatron.

FIG. 6. Variation of ECR zone in both side views of the launcher as a function of $B_{applied}$.

FIG. 7. Effect of $p$ on a hydrogen plasma produced by the source shown in Fig. 5.

FIG. 8. Effect of $p$ on an argon plasma. A uniform plasma can be produced at 6.4 mTorr.

FIG. 9. Radial profile of an oxygen plasma produced for etching experiments.

FIG. 10. Etching profiles of photoresist/silicon in an oxygen plasma with a radial profile as shown in Fig. 9.

ORNL-DWG 75-11295R

| | $I_{SM}$ (A) | $I_{AUX}$ (A) | $I_{ARC}$ (A) | $\Delta n/r_g$ (±%) | $\frac{\Delta n}{n}$ (±%) |
|---|---|---|---|---|---|
| ● | 70 | 5.4 | 250 | 20 | 10 |
| ○ | 50 | 0 | 325 | 2 | 5 |

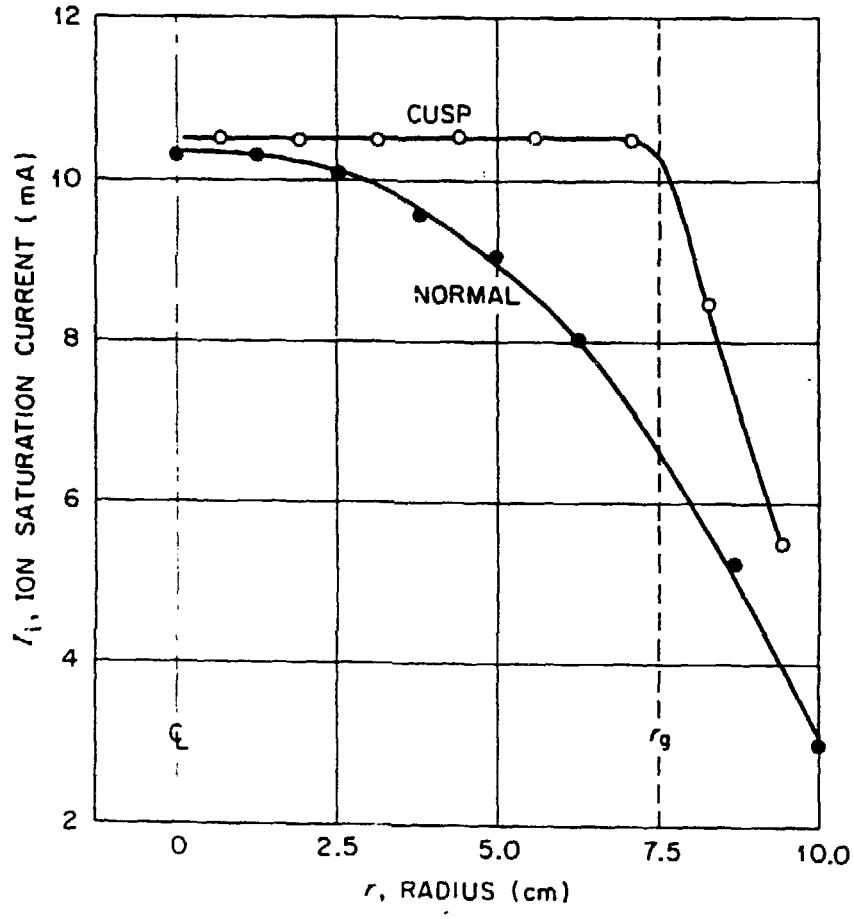

ORNL-DWG 89-2313 FED

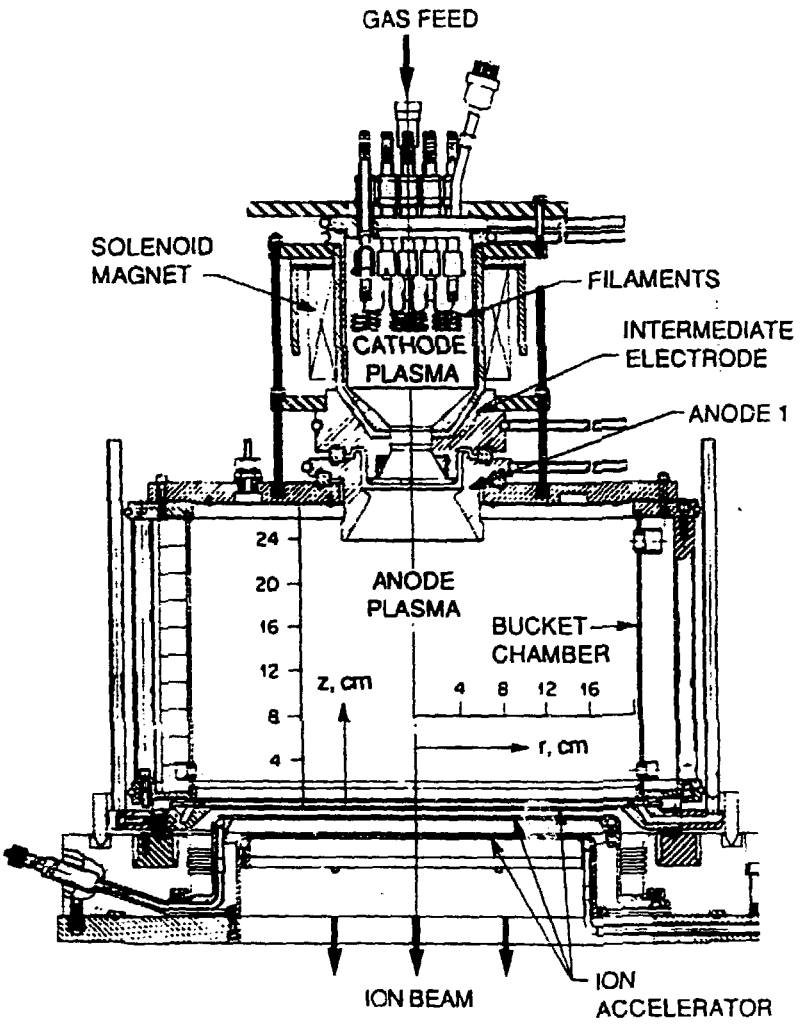

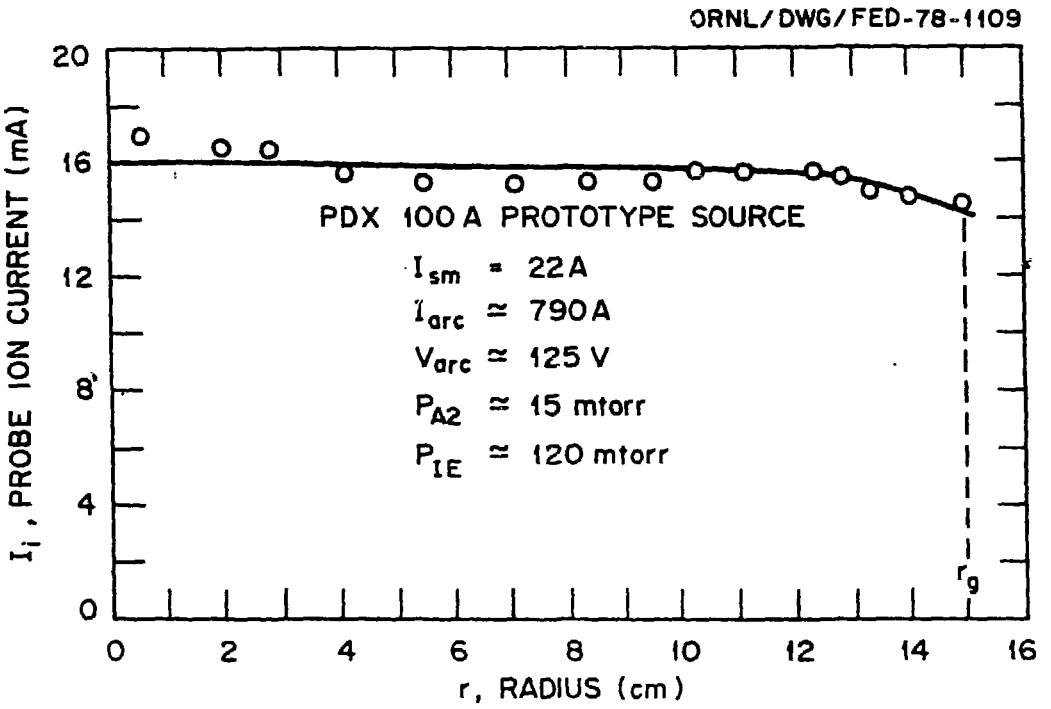
ORNL/DWG/FED-78-1109
20
16
12
8
4
0
$I_i$, PROBE ION CURRENT (mA)
PDX 100 A PROTOTYPE SOURCE
$I_{sm}$ = 22 A
$I_{arc}$ ≃ 790 A
$V_{arc}$ ≃ 125 V
$P_{A2}$ ≃ 15 mtorr
$P_{IE}$ ≃ 120 mtorr
$r_g$
0
2
4
6
8
10
12
14
16
r, RADIUS (cm)

# CIRCULAR AND RECTANGULAR DUOPIGATRON ION SOURCE DEVELOPMENT AT ORNL

ORNL-DWG 89M-2757 FED

10 A, 10-cm-diam, 1974

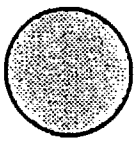

30 A, 15-cm-diam, 1975

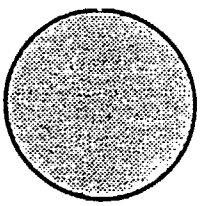

60 A, 22-cm-diam, 1976

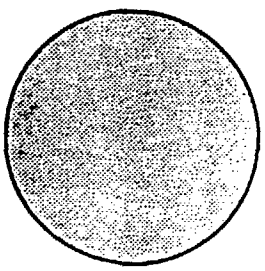

100A, 30-cm-diam, 1978-80

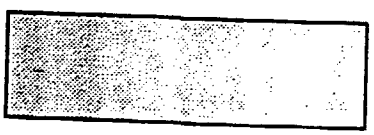

50 A, 30 s,

13 X 43 cm, 1983

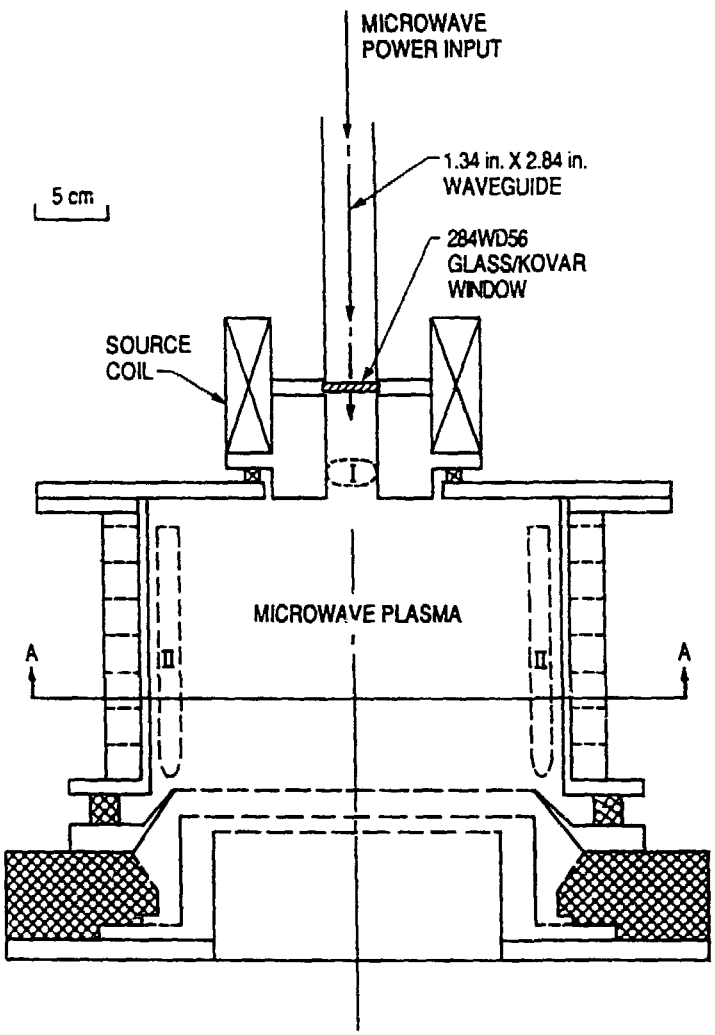
MICROWAVE
POWER INPUT
1.34 in. X 2.84 in.
WAVEGUIDE
5 cm
284WD56
GLASS/KOVAR
WINDOW
SOURCE
COIL
I
MICROWAVE PLASMA
A
II
II
A

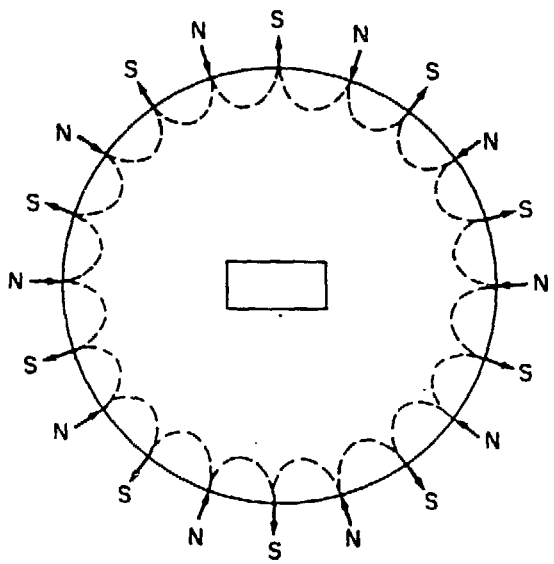
N
S
N
S
S
N
N
S
S
N
N
S
S
N
N
S
S
N
N
S
S
N
N
S

SECTION A-A

□ RESONANCE CURVE FOR $B_{MAX}$ = 1 kG

○ RESONANCE CURVE FOR $B_{MAX}$ = 2 kG

ORNL-DWG 89M-2732 FED

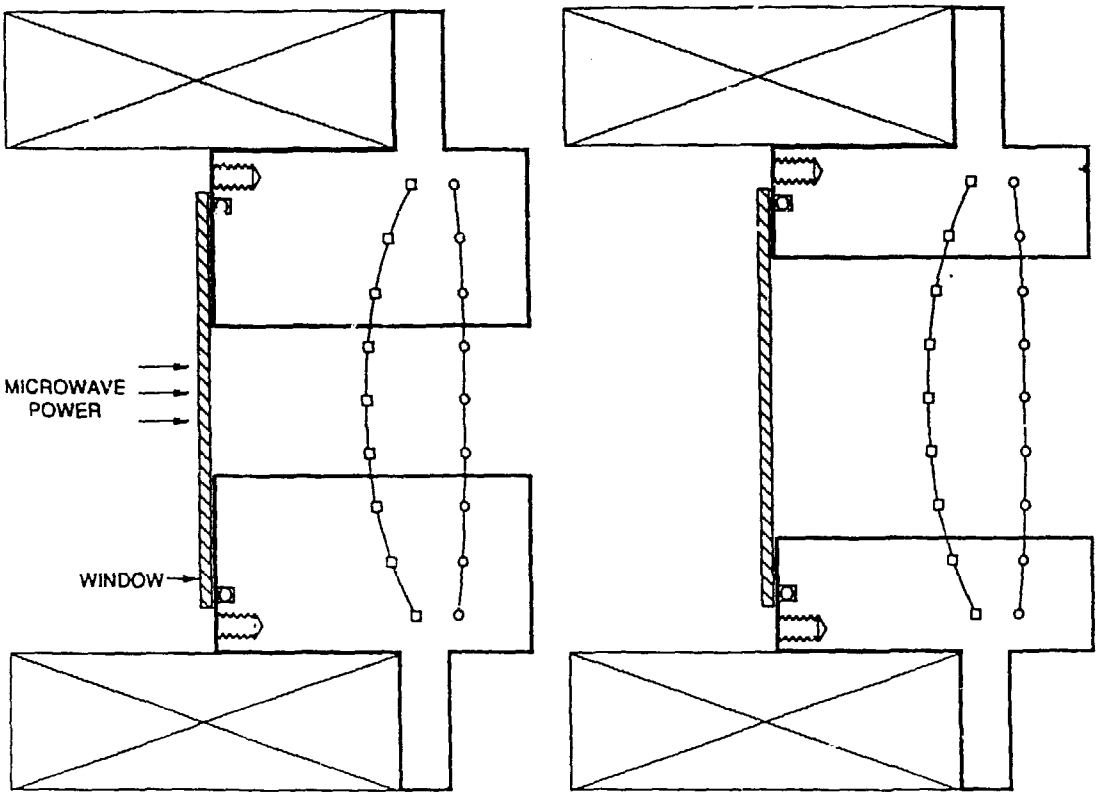

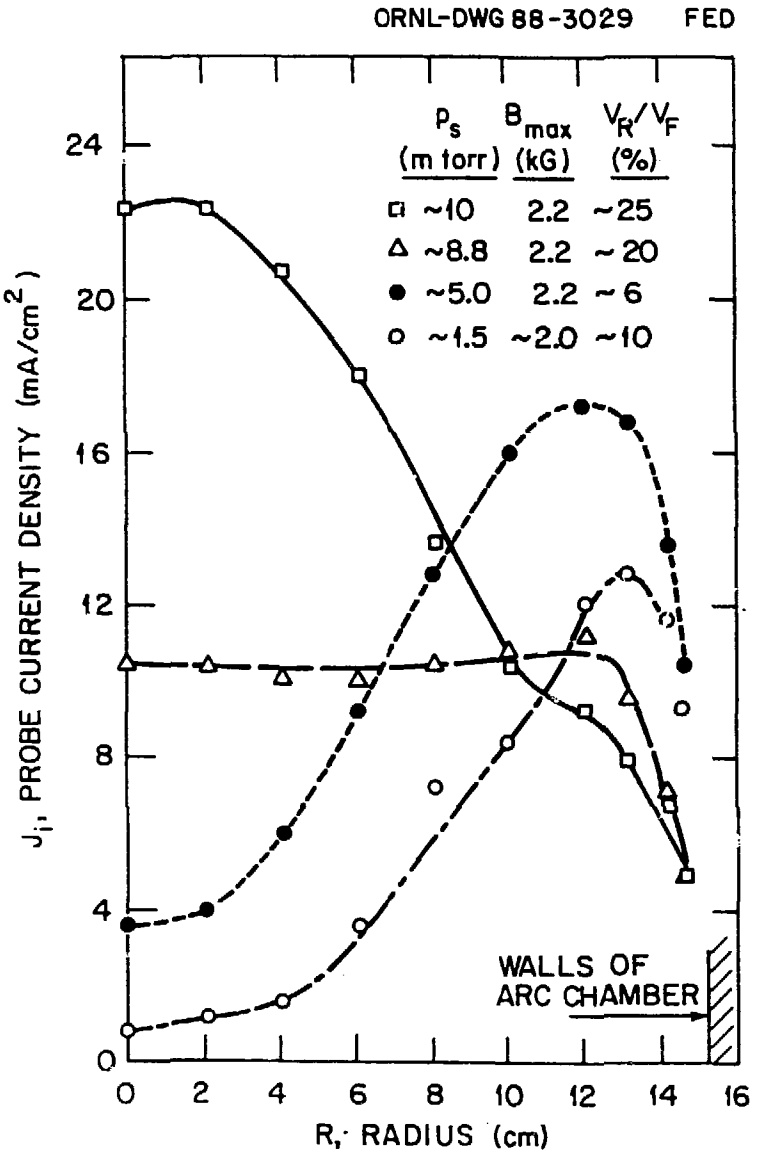
ORNL-DWG 88-3029 FED
$P_s$ (m torr)
$B_{max}$ (kG)
$V_R/V_F$ (%)
□ ~10 2.2 ~25
△ ~8.8 2.2 ~20
● ~5.0 2.2 ~6
○ ~1.5 ~2.0 ~10
WALLS OF ARC CHAMBER
$J_i$, PROBE CURRENT DENSITY (mA/cm$^2$)
R, RADIUS (cm)
0
4
8
12
16
20
24
0
2
4
6
8
10
12
14
16

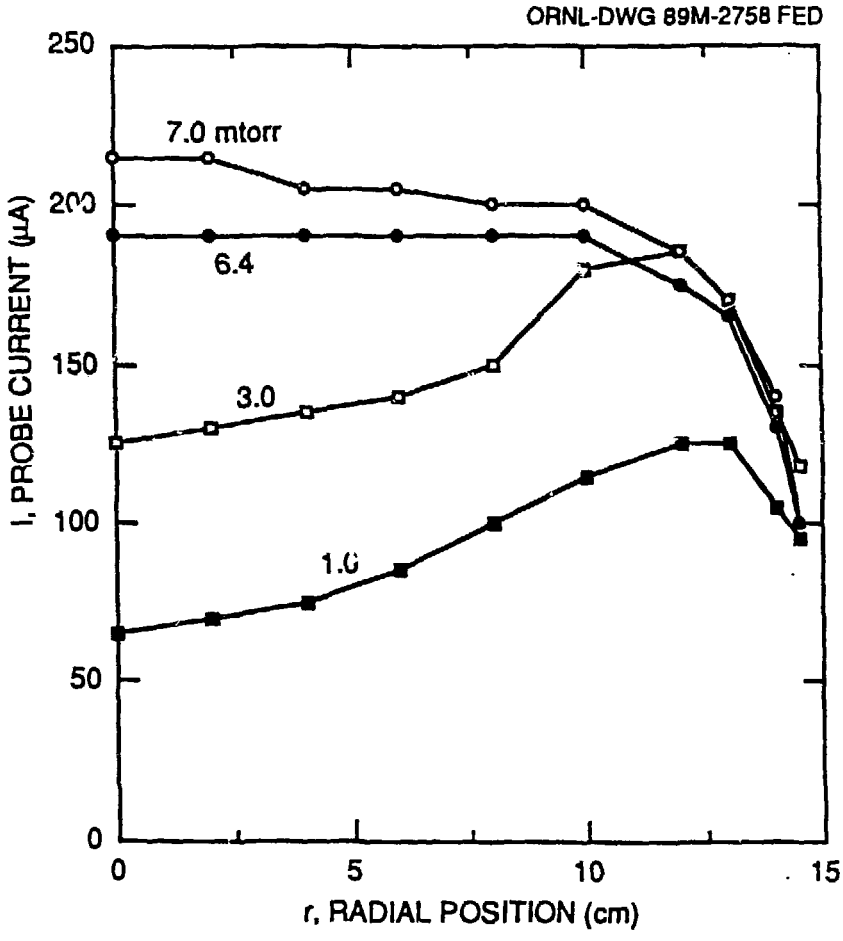
ORNL-DWG 89M-2758 FED
250
200
150
100
50
0
I, PROBE CURRENT (μA)
7.0 mtorr
6.4
3.0
1.0
0
5
10
15
r, RADIAL POSITION (cm)

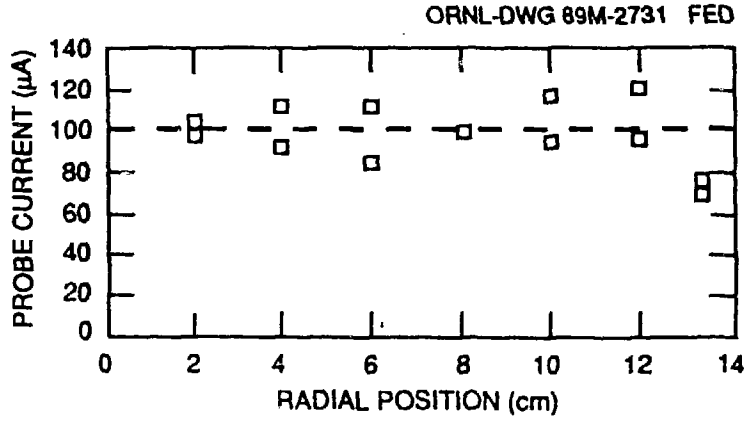
ORNL-DWG 89M-2731 FED
PROBE CURRENT (μA)
140
120
100
80
60
40
20
0
0
2
4
6
8
10
12
14
RADIAL POSITION (cm)

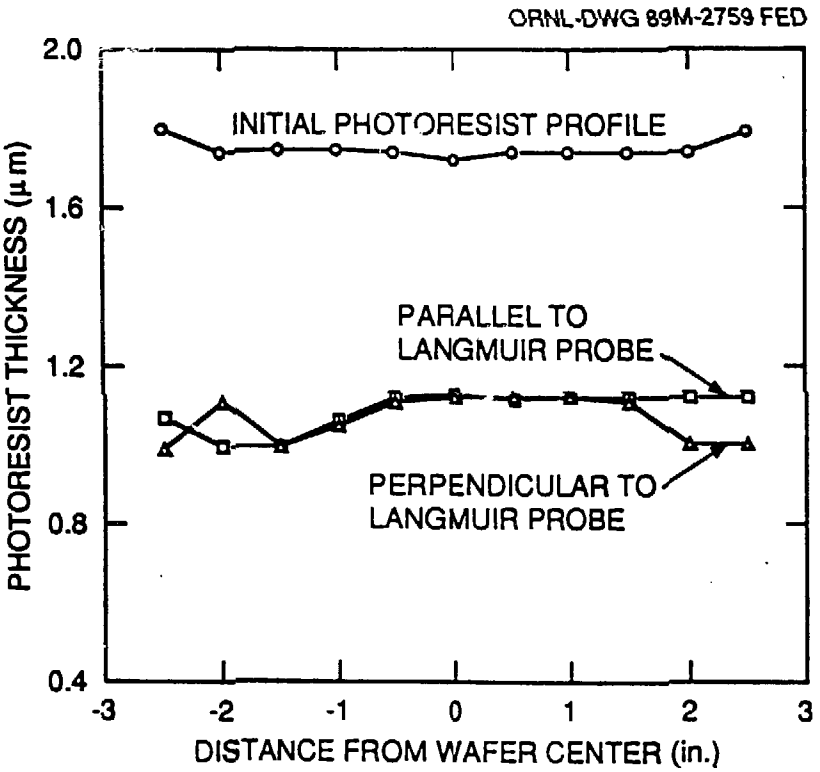
ORNL-DWG 89M-2759 FED
2.0
1.6
1.2
0.8
0.4
PHOTORESIST THICKNESS (μm)
INITIAL PHOTORESIST PROFILE
PARALLEL TO
LANGMUIR PROBE
PERPENDICULAR TO
LANGMUIR PROBE
-3
-2
-1
0
1
2
3
DISTANCE FROM WAFER CENTER (in.)